Biointerface Research in Applied Chemistry
Open-Access Journal (ISSN: 2069-5837)

Article
Volume 13, Issue 6, 2023, 503
https://doi.org/10.33263/BRIAC136.503

Transitions Among Doped *GaAs* Quantum Dot Eigenstates Initiated by Time-Varying Impurity Potential: Influence of Noise

Swarnab Datta [1], Sekh Mohammed Arif [2], Debi Roy [3], Manas Ghosh [2,*]

[1] Eklavya Model Residential School, Kanksa, West Burdwan-713148, West Bengal, India
[2] Department of Chemistry, Physical Chemistry Section, Visva-Bharati University, Santiniketan, Birbhum 731 235, West Bengal, India; arif8talpur@gmail.com(S.M.A.);pcmg77@rediffmail.com (M.G.);
[3] Department of Chemistry, Abhedananda Mahavidyalaya, Sainthia, Birbhum 731234, West Bengal, India
* Correspondence: pcmg77@rediffmail.com(M.G.);

Scopus Author ID 8258661600

Received: 18.10.2022; Accepted: 24.11.2022; Published: 31.01.2023

Abstract: The study thoroughly analyzes the time-average excitation rate of impurity-doped *GaAs*quantum dots under the supervision of Gaussian white noise. The excitation of the ground state population has been initiated by a time-dependent impurity potential strength. Gaussian whitenoise links with the system by additive and multiplicative modes. The study unveils the outcomeof some parameters' concerted impact, which ultimately designs the characteristics of the timeaverageexcitation rate plots. These parameters include a variation of several physical quantities andtheir magnitude, the presence of Gaussian white noise in a given mode, and the time-dependent fluctuation of impurity potential strength (periodic/random). As a result, the time-average excitation rate diagramsconsist of monotonic growth, monotonic drop, maximization (importantgiventhe production of large nonlinear optical properties), and minimization and saturation (relevant to dynamic freezing). The observations highlight the means of exploiting time-dependent impuritypotential strength to regulate the time-average excitation rate among the doped *GaAs* quantumdot eigenstates.

Keywords: quantum dot; Gaussian white noise; time-average excitation rate; time-dependent impuritypotential strength.

1. Introduction

Quantum dots (QDs) are a special class of low-dimensional nanostructures characterized by the completely restricted motion of the carriers (electrons and holes) in space. By virtue of their extremely small size, they become able to exhibit a number of quantum phenomena. QDs manifest remarkable size-dependent electronic, electrical, optical, magnetic, and thermodynamic properties. These properties are often found to be quite tunable and lead to widespread usage of QDs in various technologically advanced devices.

Doping of impurity to QD affects its effective confinement potential (ECP) and altersits energy spectrum and eigenstates. The above alteration makes external regulation ofthe physical properties of QDs quite achievable, giving rise to the enormous scope of fabricatingadvanced quantum devices. As a result, we find lots of research works examining the impurity effects in QD and other low-dimensional semiconductor systems (LDSS) [1-10].

Gaussian white noise (GWN) can be made a component of the ECP when it is appliedto the doped QD. Noise merits relevance since it recognizably influences the output of QD-baseddevices. Noise function can be thought to be consisting of two notable features,zero-average, and spatial delta-correlation. Moreover, the inclusion of noise inthe system can be accomplished via two different roadways, viz. additive and multiplicative. These two roadways, in effect, lead to different types of system-noise coupling and hence to varyingmagnitudes of system-noise interplay compared with the environment without noise.

Promoting the electronic probability of the lowest energy state to the excited states in QDs opens up new avenues of electronic transport, designing novel optoelectronic and light-emitting devices and quantum computation [11-13]. Such promotions are often carried outby the interaction of low-dimensional systems with incoming electromagnetic radiation [13-18]. The intensity of the above transition is dictated by the ECP of QD. Aforesaid interactionalso leads to the generation of noticeable linear and nonlinear optical (NLO) responses of low-dimensional systems [19-43]. However, instead of invoking any external field, the aboveexcitation can also be initiated by an impurity (dopant) where the impurity potential strength(IPS) becomes time-dependent, V_0(t). The time-variation of the IPS has been assumed to beperiodic as well as random about its value immediately before the onset of time-evolution,i.e., V_0(0). Such time-variation could generate from the environment inside the crystal latticethat encompasses the doped QD. The said ambiance could over periodic or random thruststo the doped QD, thereby causing aforesaid time-variation.

The present study involves a 2-d QD (GaAs) where a lone electron suffers from a restricted motion over the x - y plane by a lateral parabolic potential with a vertical magnetic field. The QD incorporates Gaussian impurity as the dopant and is further subject toapplied GWN. Therefore, the inherent confinement potential of QD, the dopant (impurity)potential, and GWN become the components of the ECP. Now, the timedependence of IPShas been invoked (periodic as well as random), which initiates the shifting of the ground stateelectronic population to all the excited states. The study endeavors to monitor the time-average excitation rate (TAER) features of doped QD. In some of our recent works, TAERhas been thoroughly explored, where the driving forces behind the population transfer come out to be totally different from the present context [44-46]. Thus, the present work becomesabsolutely independent and uncorrelated with the works mentioned above. It becomes evidentthat any change in the physical quantities that could perturb the ECP would, in consequence, affect the TAER. The said physical quantities comprise of magnetic field (B),confinement potential (ω_0), dopant location (r_0), the initial value of IPS [V_0(0)], binding energy(BE), aluminum concentration (x) (for doped $Al_xGa_{1-x}As$ QD) [30], noise strength (ζ), position-dependent effective mass (PDEM) [47-55], position-dependent dielectric screeningfunction (PDDSF) [47, 49, 56, 57], geometrical anisotropy [58-61], hydrostatic pressure (HP)[27, 33, 62, 63] and temperature (T) [27, 62, 63]. The present inquiry makes a meticulous effortto elucidate the attributes of TAER plots of doped QD, under the combined influence ofvarying physical parameters, GWN, and the time-dependent IPS.

2. Method

The QD Hamiltonian containing the dopant and GWN reads

$$H_0 = H_0' + V_{imp}(0) + \xi(x,y). \quad (1)$$

The dopant-free QD is represented by the HamiltonianH_0', which, under effective mass approximation, reads

$$H_0' = \frac{1}{2m^*}\left[-i\hbar\nabla + \frac{e}{c}\vec{A}\right]^2 + \frac{1}{2}m^*\omega_0^2(x^2+y^2)\,. \quad (2)$$

H_0' consists of the lateral parabolic confinement $V_{conf}(x,y) = \frac{1}{2}m^*\omega_0^2(x^2+y^2)$,$\omega_0$ and m^* are the confinement frequency and the effective mass of the electron, respectively. The vector potential A, in the Landau gauge, is given by [A = (By, 0, 0)], where B is the magnetic field strength. H_0' can alternatively be written as

$$H_0' = -\frac{\hbar^2}{2m^*}\left(\frac{\partial^2}{\partial x^2}+\frac{\partial^2}{\partial y^2}\right) + \frac{1}{2}m^*\omega_0^2x^2 + \frac{1}{2}m^*\Omega^2y^2 - i\hbar\omega_c y\frac{\partial}{\partial x}\,, \quad (3)$$

where ω_c(=$\frac{eB}{m^*c}$) and Ω (=$\sqrt{\omega_0^2+\omega_c^2}$) are the cyclotron frequency and the gross confinement frequency in the y-direction, respectively. The strength of the magnetic field can be regulated by varying ω_c.

The initial (t = 0) Gaussian impurity (dopant) potential $V_{imp}(0)$ of eqn(1) comprises of three parameters of relevance and looks like

$$V_{imp}(0) = V_0(0)e^{-\gamma[(x-x_0)^2+(y-y_0)^2]}\,. \quad (4)$$

Here (x_0, y_0), $V_0(0)$, and γ stand for the coordinates of the dopant, the initial value (t = 0) of IPS, and an estimate of the spatial domain over which the dopant possesses some meaningful impact, respectively.γ is somewhat related tothe dielectric constant (ε) of the medium.

ξ (x, y) of eqn(1) incorporates the noise contribution and is endowed with zero-mean and spatial δ-correlation conditions. The following function $g(x,y)$ mathematically formulates the above characteristics as

$$\langle g(x,y)\rangle = 0 \quad (5)$$

and

$$\langle g(x,y)g(x',y')\rangle = 2\zeta\delta[(x,y)-(x',y')]\,, \quad (6)$$

respectively, with ζ as the noise strength. The function $g(x,y)$exhibiting a Gaussian distribution can be generated with the help of the Box-Muller algorithm. The noise function ξ(x, y) is said to be additive and multiplicative based on the manner by which its links with the doped QD. The additive white noise (ADWN) and multiplicative white noise (MLWN) connect ξ(x, y) with $g(x,y)$as given below:

$$\xi(x,y) = \lambda_1 g(x,y), \quad \text{in the case of ADWN} \quad (7)$$

and

$$\xi(x,y) = \lambda_2 g(x,y)(x+y), \text{ in the case of MLWN.} \quad (8)$$

where λ_1 and λ_2 are two arbitrary parameters.

The solution of the time-independent Schrödinger equation has been carried out by adopting the variational strategy. The required trial function $\psi_k(x,y)$ for this purpose has been selected to be the direct product of harmonic oscillator eigenfunctions. Thus,

$$\psi_k(x,y) = \sum_{nm} C_{nm,k}\phi_n(px)\phi_m(qy), \quad (9)$$

where $c_{nm,k}$ are the linear superposition coefficients and $p = \sqrt{\frac{m^*\omega_0}{\hbar}}$ and $q = \sqrt{\frac{m^*\Omega}{\hbar}}$. Now, the construction of the Hamiltonian matrix for H_0 [cf. eqn(1)] and its consequent diagonalization lead to the obtainment of the normalized eigenvectors and the energy eigenvalues.

The time-dependent IPS, V_0(t), about its initial value, V_0(0), can be written as

$V_0(t) = V_0(0)\cos(\nu t)$, for periodic change

$= V_0(0)R(t)$, for random change, (10)

where ν is the fluctuation frequency of IPS and R(t) is the time-varying random number. As a result, the overall impurity potential changes with time and reads [cf. eqn(4)]

$V_{imp}(\mathrm{t}) = V_0(\mathrm{t})e^{-\gamma[(x-x_0)^2+(y-y_0)^2]}$

$= V_{imp}(0)\cos(\nu t)$,for periodic change

$= V_{imp}(0)R(t)$,for random change. (11)

Thus, the time-varying Hamiltonian becomes [cf. eqn(1)]

$H(t) = [H_0 - V_{imp}(0)] + V_{imp}(t)$. (12)

The matrix elements linking any two arbitrary eigenstates of H_0 [cf. eqn(1)] are determined involving V_{imp}(t). Next, the time-evolving wave function $\Psi(t)$(due to the fluctuating IPS) has been expanded as a superposition of the H_0 eigenfunctions viz.

$$\Psi(x,y,t) = \sum_q a_q(t)\psi_q(x,y), \quad (13)$$

and the associated time-dependent Schrödinger equation (TDSE) viz.

$i\hbar\frac{\partial\Psi}{\partial t} = H\Psi$or equivalently

$i\hbar\dot{a}_q(t) = Ha_q(t)$. (14)

Was integrated by the sixth-order Runge-Kutta-Fehlberg method. The time-dependent coefficients, i.e., a_q(t)s vary under the initial conditions $a_0(0) = 1$ and $a_q(0) = 0$; $\forall q \neq 0$, where q is the H_0 eigenstate. The choice of initial conditions indicates the total accumulation of the electronic population absolutely to the lowest energy level before the onset of time-propagation. Immediately after the IPS starts fluctuating with time, the electronic population begins to get distributed among the various excited states. The time-dependent probability of any arbitrary k^{th} eigenstate of H_0 is given by the quantity $P_k(t) = |a_k(t)|^2$. Naturally, the quantities $Q(t) = 1\text{-}P_0(t)$ and $R_{ex}(t) = \frac{dQ}{dt}$ stand for the amount of excitation and the rate of excitation with the progress of time, respectively. Lastly, the time-average excitation rate (TAER) due to the time-changing IPS reads $\langle R_{ex}\rangle = \frac{1}{T}\int_0^T R_{ex}(t)dt$, with T being the entire time of timeevolution.

3. Results and Discussion

In a general sense, the various physical parameters used for the GaAs QDs assume the following values: ε = 12.4 and m^* =0.067m_0, where m_0 is electron mass in a vacuum, $\hbar\omega_0$= 100.0 meV, B = 5.0 T, $V_0(0)$ = 200.0 meV, r_0 = 0.0 nm and ζ = 1.0× 10^{-4}, respectively.

3.1. Role of magnetic field (B) and confinement potential (ω_0).

Figure 1a shows the TAER plots with changes in the magnetic field strength in the absence and presence of noise, both for periodic and random changes of IPS. In the case of periodic variation, under a noise-free state, the TAER plot exhibits a declining trend with an

increase in *B*. The said plot, under applied ADWN, reveals an increasing trend with an increase in *B*. The TAER profile, under MLWN, depicts prominent maximization at *B*~5.3 T. Added to this, the said profiles also exhibit a sort of saturation at large *B* in the absence of noise and under-applied ADWN.

For a random variation of IPS, the TAER plot divulges maximization at *B*~ 4.7 T without noise. The said plot, under ADWN, exhibits persistent increase with increase as *B* enhances up to *B*~ 3.3 T and saturates thereafter. And in the case of MLWN, the TAER plot unveilsminimization at *B*~ 4.2 T. We observe saturation in the TAER profiles at large magnetic field strength in all the cases.

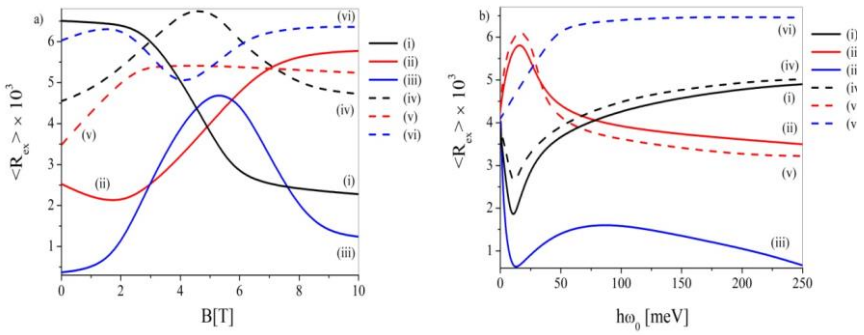

Figure 1.TAER diagrams against **(a)***B*, **(b)***hω*$_0$: For all diagrams**(i)** devoid of noise and periodic variation of IPS, **(ii)** presence of ADWN and periodic variation of IPS, **(iii)** presence of MLWN and periodic variation of IPS, **(iv)** noise-free state and random variation of IPS, **(v)** presence of ADWN and random variation of IPS and **(vi)** presence of MLWN and random variation of IPS.

Figure 1b delineates the analogous diagrams against the variation of the confinement potential. For the periodic change of IPS, the TAER profile, without noise, exhibits *minimization* at $h\omega_0$ ~ 10.4 meV. The profile displays a sort of saturation at a strong confinement regime aswell. In the presence of ADWN, we observe *maximization* at $h\omega_0$~ 16.4 meV and a kind of saturation, again at a strong confinement regime. The presence of MLWN gives rise to *minimization* in the TAER plot at $h\omega_0$ ~ 13 meV.

During the random variation of IPS, the TAER profiles show qualitative resemblance with their periodic counterparts in the absence of noise and with ADWN. Even the locations of *minimization* and *maximization* remain nearly the same. However, under applied MLWN, the TAER plot depicts steady enhancement with an increase in ω_0 up to $h\omega_0$~ 74 meV and saturates thereafter with further increase in ω_0.

3.2. Role of Role of dopant location (r_0), initial value of dopant potential strength [$V_0(0)$] and binding energy (BE).

Figure2a delineates the similar profiles monitored against the variation of dopant location. During the periodic change of IPS and without noise, the TAER plot undergoes a steady fall, shifting the dopant to more and more off-center positions. The plot finally exhibits saturation for far-off-center dopants. The TAER profiles evince *maximization* at r_0 ~ 9.6 nm and r_0~ 5.6 nm with ADWN and MLWN, respectively.

The observations change a lot when IPS fluctuates randomly with time. In this case, under noise-free conditions and with ADWN, the TAER profiles exhibit some initial

oscillations and culminate in saturation for far-off-center dopants. In the presence of MLWN, however, the TAER profile at first increases monotonically up to r_0~ 7.4 nm and then becomes steady with a further shift of the dopant.

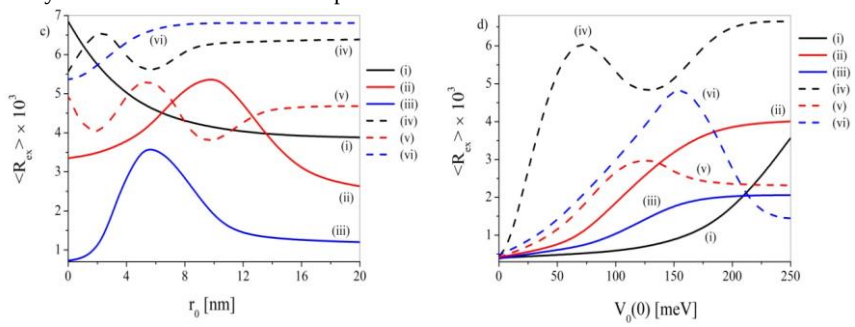

Figure2: TAER diagrams against **(a)** r_0 and **(b)** $V_0(0)$: In all the plots **(i)** noise-free state and periodic variation of IPS, **(ii)** presence of ADWN and periodic variation of IPS, **(iii)** presence of MLWN and periodic variation of IPS, **(iv)** noise-free state and random variation of IPS, **(v)** presence of ADWN and random variation of IPS and **(vi)** presence of MLWN and random variation of IPS.

Commented [AGN1]: Figure 2. Figure numbers are revised

Figure2b manifests the TAER profiles following a change in the initial value of IPS. Such a change indicates a gradual shift from a dopant-free QD to QD doped with more and more strong impurity potential. For the periodic change of IPS, both in the presence and absence of noise, the TAER profiles discern an increasing trend with an increase in $V_0(0)$. However, the extent of increase happens to be most in the absence of noise, and the TAER profiles reveal noticeable saturation at large $V_0(0)$ only in the presence of noise.

For a random variation of IPS, one observes consecutive maximization and minimization at $V_0(0) \sim 72$ meV and $V_0(0) \sim 127$ meV, respectively, under a noise-free state. On the other hand, the said profiles evince maximization around $V_0(0) \sim 128$ meV and $V_0(0) \sim 155$ meV under applied ADWN and MLWN, respectively.

The binding energy (BE) of the ground statecan be envisaged as the difference in the energies of this state with and without impurity doping. The TAER diagrams pursuing the change in BE emerges to be characteristically near to the TAER profiles following the change of $V_0(0)$ under different situations. We, thus, refrain from showingthese plots to keep the description short.

3.3. Role of aluminium concentration (x) and geometrical anisotropy (η).

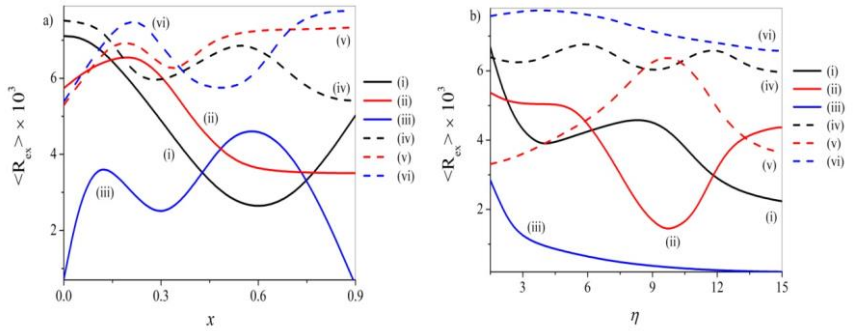

Figure 3: TAER diagrams against **(a)** x and **(b)** η: In all the plots **(i)** noise-free state and periodic variation of IPS, **(ii)** presence of ADWN and periodic variation of IPS, **(iii)** presence of MLWN and periodic variation of IPS, **(iv)** noise-free state and random variation of IPS, **(v)** presence of ADWN and random variation of IPS and **(vi)** presence of MLWN and random variation of IPS.

Commented [AGN2]: Figure 3

Figure3a demonstrates the TAER diagrams as the *Al* concentration (x) changes over a range. For this purpose,$Al_xGa_{1-x}As$ QD was considered whose effective mass reads $m^* = (0.067 + 0.083x)m_0$ [30]. In case of periodic change of IPS, without noise, the TAER profile displays *minimization* at $x \sim 0.6$. In the presence of ADWN, the said profile shows a very faint *maximization* at $x \sim 0.2$ followed by a rapid decrease with an increase in x up to ~ 0.6.With a further increase in x, the TAER registers a steady value whatsoever. The said profile, under applied MLWN, displays successive *maximization* at $x \sim 0.12$ and at $x \sim 0.58$.

Commented [AGN3]: Figures should be added near the first time they are cited, after being mentioned in the main text.
Please revise figure positioning according to this rule in the entire manuscript

When the IPS varies randomly with time, under a noise-free state, we observe consecutive *minimization* and *maximization* at $x \sim 0.3$ and $x \sim 0.54$, respectively. The TAER profile, on the other hand, depicts successive *maximization* and *minimization* at $x \sim 0.19$ ($x \sim 0.21$) and $x \sim 0.33$ ($x \sim 0.48$), respectively, under the influence of applied ADWN (MLWN). Only in the case of ADWN prominent saturation in the TAER profile is observed beyond $x \sim 0.6$.

In Figure3b we monitor the TAER diagrams againstthe geometrical anisotropy of the doped QD, reflected through the parameter $\eta = \frac{\Omega}{\omega_0}$ [cf. eqn(3)] [58, 59]. During the periodic change of IPS, without noise, the TAER diagram exhibits an overall decreasingpattern as η enhances,consisting of successive minimization and maximization at $\eta \sim 4.0$ and $\eta \sim 8.5$, respectively. The said profile displays prominent minimization at $\eta \sim 9.8$ under the sway of ADWN. In the presence of MLWN, the TAER plot manifests a steady decline with an increase in η and finally saturates at large η.

When the IPS varies randomly with time, in the absence of noise, the TAER profile exhibits undulations over the whole range of η. Distinct *maximization* in the TAER plot is observed at $\eta \sim 9.7$ in the presence of ADWN. On the other hand, under MLWN, the TAER profile evinces a net, almost regular, decreasing trend with an increase in η.

3.4. Role of the position-dependent effective mass (PDEM) and position-dependent dielectric screening function (PDDSF).

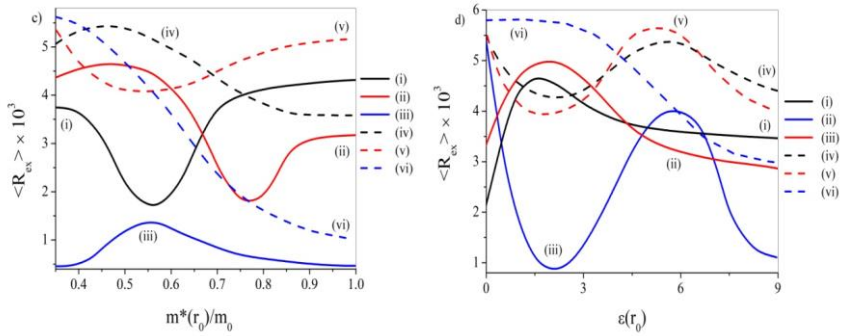

Figure 4: TAER diagrams against **(a)** $m^*(r_0)$ and **(b)** $\varepsilon(r_0)$: In all the plots **(i)** noise-free state and periodic variation of IPS, **(ii)** presence of ADWN and periodic variation of IPS, **(iii)** presence of MLWN and periodic variation of IPS, **(iv)** noise-free state and random variation of IPS, **(v)** presence of ADWN and random variation of IPS and **(vi)** presence of MLWN and random variation of IPS.

Commented [AGN4]: Figure 4

The discussions hitherto made consider the fixed effective mass (FEM) of the electron. However, the m^* can also be dependent on dopant coordinate (r_0), whence it is called PDEM and is denoted as $m^*(r_0)$ [47, 49]. Figure4a describes the TAER plots with the change in PDEM. During the periodic change of IPS, the TAER plots divulge prominent minimization at $m^*(r_0) \sim 0.56$ and at $m^*(r_0) \sim 0.76$ without noise and with ADWN, respectively. The said plot reveals maximization at $m^*(r_0) \sim 0.56$ under MLWN. On all occasions, saturationin TAER profiles is envisaged at large PDEM.

As the IPS undergoes random change with time, the TAER plots, without noise and with MLWN, exhibit a steady fall with an increase in PDEM. The said plot, under ADWN, displays minimization at $m^*(r_0) \sim 0.53$. The TAER plots, only under the influence of noise, manifest saturation at large PDEM.

Analogous to FEM, the study so far considers the static dielectric constant (SDC) of the medium. However, quite similar to PDEM, the dielectric constant may assume some sort of functional dependence on the dopant location and is consequently said to be a position-dependent dielectric screening function (PDDSF) [$\varepsilon(r_0)$] [47, 49, 56, 57]. Figure4b demonstrates the TAER profiles over a range of PDDSF. As the IPS varies periodically with time, the TAER plots exhibit maximization at $\varepsilon(r_0) \sim 1.6$ and $\varepsilon(r_0) \sim 1.9$, under a noise-free situation and in the presence of ADWN, respectively. The plots also show saturation at large values of PDDSF. The shape of the plot considerably changes with MLWN as the TAER profile now shows successive minimization and maximization at $\varepsilon(r_0) \sim 2.1$ and $\varepsilon(r_0) \sim 5.8$, respectively.

Successive *minimization* and *maximization* in the TAER profiles are again observed during the random variation of TAER, but without noise and with ADWN. They are now found at $\varepsilon(r_0) \sim 2.2$ [$\varepsilon(r_0) \sim 1.8$] and $\varepsilon(r_0) \sim 5.7$ [$\varepsilon(r_0) \sim 5.3$], respectively, under noise-free state [ADWN]. However, under MLWN, the TAER plot reveals a steady drop with an increase in PDDSF.

3.5. Role of hydrostatic pressure (HP) and temperature (T).

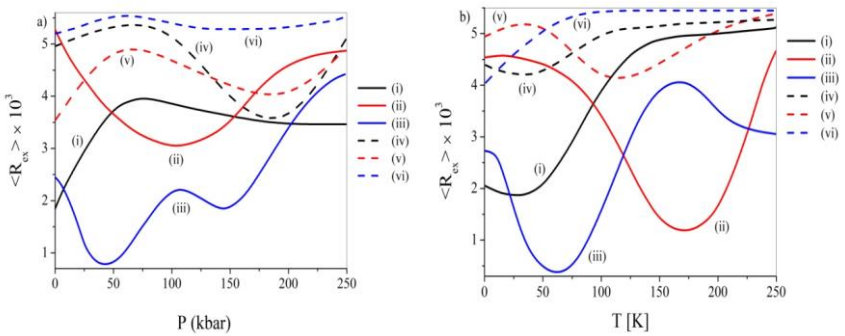

Figure 5: TAER diagrams against **(a)** *P* and **(b)** *T*: In all the plots **(i)** absence of noise and periodic variation of IPS, **(ii)** applied ADWN and periodic variation of IPS, **(iii)** applied MLWN, and periodic variation of IPS, **(iv)** absence of noise and random variation of IPS, **(v)** applied ADWN and random variation of IPS and **(vi)** applied MLWN and random variation of IPS.

Commented [AGN5]: Figure 5

Taking into account the pressure and temperaturevariation of m* and ε is necessary to analyze the role played by HP and temperature [63]. Figure5a delineates the TAER profiles as the HP varies over a range. For the periodic variation of IPS, in the absence of noise, the plot

depicts a steady rise of TAER up to P ~ 76 kbar, beyond which it registers a steady value with a further increase in pressure. The said plot shows *minimization* at P ~ 104 kbar with ADWN. In the presence of MLWN, the TAER plot depicts an overall rising trend with an increase in HP consisting of undulations.

While the IPS varies randomly with time and without noise, the TAER diagramreveals minimization at P ~ 187 kbar. Under ADWN, the said plot exhibits feeble successive maximization and minimization at P ~ 66 kbar and at P ~ 187 kbar, respectively. However, in the presence of MLWN, the TAER plot discerns a nearly steady pattern over the entire range of HP.

Figure5b represents the temperaturedependence of the TAER profiles. During the periodicvariation of IPS, without noise, the TAER increases as the temperature areraised and settleto some steady value when the temperature becomes quite high. The said plot shows minimization at T ~ 172 K under applied ADWN. Under applied MLWN, the TAER plot exhibits consecutive minimization and maximization at T ~ 62 K and at T ~ 167 K, respectively.

During the random variation of IPS, without noise and under MLWN, initially, the TAER plots increase steadily with T, followed by saturation within the moderate to the high-temperature domain. However, the TAER plot undergoes minimization at T ~ 117 K under applied ADWN.

3.6. Role of noise strength (ζ).

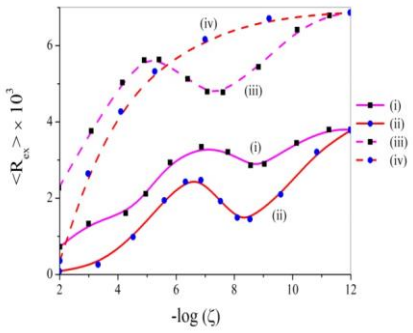

Figure 6: TAER diagrams against -log(ζ): **(i)** ADWN and periodic variation of IPS, **(ii)** MLWN and periodic variation of IPS, **(iii)** ADWN and random variation of IPS, and **(iv)** MLWN and random variation of IPS.

Commented [AGN6]: Figure 6

The sole impact of noise on the TAER plots can be realized by changing the noise strength over a range for fixed values of all other quantities. Figure6 discerns the TAER diagrams with the change of ζ under ADWN and MLWN. For the periodic variation of IPS, both under ADWN and MLWN, TAER profiles manifest a rising trend with a drop in the noise strength. However, during the said rise, both for ADWN and MLWN, *maximization* is found in the TAER profiles in the vicinity of $\zeta \sim 10^{-7}$. As the noise strength becomes extremely small, the TAER also approaches the noise-free value.

As the IPS undergoes random change, both under ADWN and MLWN, the TAER again exhibits a rising trend as ζ decreases and approaches the noise-free value for extremely small values of the noise strength. However, whereas under MLWN, the rise of TAER with a fall in ζ emerges to be absolutely monotonic, under ADWN, the TAER displays successive maximization and minimization in the neighborhood of $\zeta \sim 10^{-5}$ and $\zeta \sim 10^{-7.5}$, respectively.

Maximization of TAER deems technological importance so far as the generation of NLO properties of QDs isconcerned. The above analysis reveals the nature of the timevariation of IPS, the associated mode of application of noise, and the noise strength domain, which would be advantageous for the maximization of TAER.

3.7. Physical explanation of the outcomes.

The TAER plots following the change of various physical parameters manifest steadfast increase, steadfast fall, maximization, minimization, and saturation. These attributes appear as an outcome of the combined impact of the particular physical parameter being varied, the domain of its magnitude, the introduction of noise and its pathway (additive/multiplicative), and the type of time-dependence (periodic/random) of the IPS. TAER, in effect, indicates how the time-dependent variation of IPS regulates the time-average rate of dissemination of the lowest energy state electronic accumulation among all higher energy levels. The said dissemination occurs through the entire course of time-propagation. The maximization and minimization of TAER highlight the resultant physical atmosphere, which would be conducive and non-advantageousto the said population shift, respectively, to the largest extent. In addition to this, the steadfast growth and decay of TAER reflect parallel surges and lulls in the population shift, respectively. Moreover, the occurrence of saturation in the TAER diagrams points to a consistent population shift (dynamic freezing) and is mainly found when the different physical quantities assume a medium to large values. Thus, the quantitative measure of the population excitation among the higher states, i.e., the TAER, significantly depends on the environment. Modulation of the environment, therefore, also modulates the TAER.The said modulation appears to be a combined outcome of the varying physical quantity over some specific range, noise along with its roadway of application, and the nature of timefluctuation of the IPS.

From another perspective, the TAER appears to be a quantitative estimate of how the various eigenstates undergo some sort of average mutual overlap throughout the whole period of timepropagation. The enhancement and depletion of TAER arise out of the amplification and depletion of the above overlap, respectively. On the other hand, maximization, minimization, and saturation in the TAER diagrams reflect the largest, smallest, and steady overlap between the several eigenstates. However, the nature and extent of such overlap depend on the system's effective confinement potential (ECP). Generally,enhancement and weakening of ECP obstruct and favor such overlap, respectively. The variation of a given physical quantity and the introduction of noise (including its mode) affect the ECP to a recognizable extent and, consequently, the average overlap and TAER.

The time-varying IPS causes a continuous redistribution of the electronic population among the eigenstates. The size of the said redistribution and hence theTAER, however, depends on the pattern of the timeprogress(periodic/random). The said population redistribution originates from a change in energy with time due to the above fluctuation. The pattern of TAER profiles can be understood by observing the amount of energy, which, on average, the fluctuating IPS delivers over the time span *t*. The time-dependent energy of the system originating from the fluctuating IPS can be expressed as

$$E(t) = \sum_k E_k(0) P_k(t) \qquad (15)$$

where $E_k(0)$ is the k^{th} eigenstate energy of H_0 immediately before the onset of time-progress (i.e at $t = 0$). $E(t)$, therefore, represents the energy of the system at time t owing to the time-

varying IPS, incorporating within it the energy initially possessed by the system (i.e.,at t = 0). Initially, because of the total localization of the electronic population to the ground energy level, the system energy simply becomes the ground state energy. As soon as the IPS starts fluctuating with time, the energy also begins to change, and the population gets scattered among various excited states. Thus, these excited states now also begin to contribute to the total energy [*E(t)*]. The rate of change of average *E(t)* with time due to the fluctuating IPS has been evaluated with the help of the time-dependent Hellman-Feynman theorem as outlined below [cf. eqns(10-14)]:

$$\frac{d\langle E(t)\rangle}{dt} = \left\langle \Psi(t)\right| \frac{dH(t)}{dt} \left|\Psi(t)\right\rangle = \left\langle \Psi(t)\right| \frac{dV_{imp}(t)}{dt} \left|\Psi(t)\right\rangle. \qquad (16)$$

Thus,

$\frac{d\langle E(t)\rangle}{dt} = -\nu \sin(\nu t) \langle \Psi(t)|V_{imp}(0)|\Psi(t)\rangle$, for periodic fluctuation

$= R'(t)\langle \Psi(t)|V_{imp}(0)|\Psi(t)\rangle$,for random fluctuation, (17)

and the impurity integral over the spatial coordinates is given by [cf. eqn(13)]

$$\langle \Psi(t)|V_{imp}(0)|\Psi(t)\rangle = \sum_p \sum_q a_p^*(t) a_q(t) \langle \psi_p(0)|V_{imp}(0)|\psi_q(0)\rangle \quad (18)$$

Ψ(t) and $\psi_p(0)$s are the time-propagating wave function and the *p*-th state eigenfunction of the original unperturbed system, respectively. Hence, the time-varying IPS-induced delivery of average energy over time span *t* given by

$\langle E(t)\rangle = \langle E(0)\rangle - \nu \int_0^t \sin(\nu t') \langle \Psi(t')|V_{imp}(0)|\Psi(t')\rangle dt'$, for periodic fluctuation

$= \langle E(0)\rangle + \int_0^t \mathrm{R}'(t') \langle \Psi(t')|V_{imp}(0)|\Psi(t')\rangle dt'$,for random fluctuation.(19)

The integrations in eqn(19) are numerically carried out using Simpson's $\frac{1}{3}$rd rule.

At length, the average energy transferred by the time-varying IPS over the full time (*T*) of time-evolution reads

$$\langle E\rangle = \int_0^T \langle E(t)\rangle dt \qquad (20)$$

As representative cases, we consider the TAER profiles against the magnetic field strength, with and without noise, and both for periodic and random time-dependence of IPS [cf. (Figure 1a)]. We now determine the $\langle E\rangle$ as a function of *B* for the situations mentioned above and try to correlate the TAER plots with the $\langle E\rangle$ plots. Figure7a and Figure7b delineate the $\langle E\rangle$ vs *B* plots with and without noise for periodic and random time-dependence of IPS, respectively. For the periodic variation, under a noise-free state, the $\langle E\rangle$plot exhibits a declining trend with an increase in *B*. The said plot, under applied ADWN, reveals an increasing trend with an increase in *B*. The $\langle E\rangle$ profile, under MLWN, depicts prominent maximization at $B \sim$ 5.3 T. Added to this, the said profiles also exhibit sort of saturation at large *B* in the absence of noise and under-applied ADWN.

For a random variation of IPS, the $\langle E\rangle$ plot divulges maximization at $B \sim 4.7$ T without noise. The said plot, with ADWN, exhibits a regular increase as B enhancesup to $B \sim 3.3$ T and saturates thereafter. And in the case of MLWN, the $\langle E\rangle$plot unveils minimization at $B \sim 4.2$ T. In all the cases, we observe saturation in the $\langle E\rangle$profiles at large magnetic field strength.

Above findings suggest that the attributes of the TAER diagrams are governed bythe average energy delivered by the time-dependent IPS over the entire timepropagation. This occurs due to the appropriate modification of the underlying structures of the phase space. The

above delivery of the average energy arises out of the resultant effect of the varying physical quantity (*B* in these representative cases), absence/presence of noise, route of introduction of noise (ADWN and MLWN), and the nature of time-dependence of IPS (periodic/random).

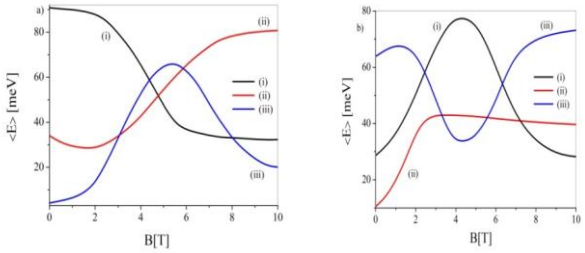

Figure 7: Plots of **(a)** ⟨*E*⟩ against *B* for periodic fluctuation of IPS and **(b)** ⟨*E*⟩ vs *B* for random fluctuation of IPS: in both the plots **(i)** noise-free condition, **(ii)** ADWN and **(iii)** MLWN.

Commented [AGN7]: Figure 7

4. Conclusions

TAER of impurity containing *GaAs* QD, initiated by time-dependent IPS, has been meticulouslyexamined under the supervision of GWN. The study reveals that the resultant influence of a few parameters evidently designs the subtleties of the TAER diagrams. Theseparameters involve the given physical property being altered (including its magnitude),the application of noise and its pathway, and the nature of the timedependenceof IPS. Aforesaid resultant influence produces steadfast rise, steadfast fall, maximization, minimization, and saturation in the TAER diagrams. Specifically, maximization and saturation are important in view of the technological demandof producing large NLO response and dynamic freezing, respectively. The inquiry sheds light on exploiting the time-dependent IPS to modulate the TAER among thedoped *GaAs* QD eigenstates. The findings appear to be relevant in view of the applicability of QD in optoelectronic devices.

Funding

This research received no external funding.

Acknowledgments

The authors S. M. A., A. B., A. G., and M. G., thank DST-FIST (Government of India)and UGC-SAP (Government of India) for support.

Conflicts of Interest

The authors declare no conflict of interest.

References

1. Baskoutas, S.; Paspalakis, E.;Terzis, A. F. Electronic structure and nonlinear optical rectification in a quantum dot: effects of impurities and external electric field.*J. Phys.: Condensed Matter* **2007**, *19*, 395024,https://doi.org/10.1088/0953-8984/19/39/395024.
2. Karabulut, I.;Baskoutas, S. Linear andnonlinear optical absorption coefficients and refractiveindex changes in spherical quantum dots: effects ofimpurities, electric field, size, and optical intensity.*J. Appl. Phys.* **2008**,*103*, 073512, https://doi.org/10.1063/1.2904860.

3. Karabulut, I.; Baskoutas, S. Second andthird harmonic generation susceptibilities of sphericalquantum dots: effects of impurities, electric field and size.*J. Computational and Theoretical Nanosci.* **2009**, *6*, 153-156, http://dx.doi.org/10.1166/jctn.2009.1020.
4. Kasapoglu, E.; Ungan, F.; Sari, H.; Sökmen, I.; Mora-Ramos, M.E.; Duque, C.A. Donor impurity states and related optical responses in triangular quantum dots under applied electric field. *Superlattices and Microstructures* **2014,** *73*, 171-184,https://doi.org/10.1016/j.spmi.2014.05.023.
5. Çakir, B.;Yakar,Y.;Özmen, A. Investigation of magnetic field effects on binding energiesin spherical quantum dot with finite confinement potential,*Chem. Phys. Lett.* **2017**,*684*, 250256,https://doi.org/10.1016/J.CPLETT.2017.06.064.
6. Baghramiyan, H. M.;Barseghyan, M. G.; Kirakosyan, A. A.;Restrepo, R. L.; Mora-Ramos, M. E.; Duque, C. A.Donor impurity-related linear and nonlinear opticalabsorption coefficients in *GaAs\Ga*$_{1-x}$*Al*$_x$*As* concentric double quantum rings: Effects of geometry,hydrostatic pressure, and aluminium concentration.*J. Lumin.***2014**, *145*,676-683, http://dx.doi.org/10.1016/j.jlumin.2013.08.061.
7. Duque, C. A.; Mora-Ramos, M. E.;Kasapoglu, E.;Ungan, F.;Yesilgul, U.;Sakiroglu, S.; Sari,H.;Sökmen, I. Impurity-related linear and nonlinear opticalresponse in quantum-well wires with triangular crosssection.*J. Lumin*. **2013**, *143*, 304-313, https://doi.org/10.1016/j.jlumin.2013.04.048.
8. Sedehi, H. R. R.; Khordad, R.; Bahramiyan, H. Optical properties and diamagnetic susceptibility of a hexagonal quantum dot. impurity effect.*Optical and Quantum Electronics* **2021**,*53*,1-11,https://doi.org/10.1007/s11082-021-02927-7.
9. Belamkadem, L.;Mommadi, O.;Boussetta, R.;Chouef, S.;Chnafi, M.;Moussaouy, A. El.;Vinasco, J. A. Laroze, D.;Duque, C. A.;Kenfack-Sadem, C.;Tsiaze, R. M. K.;Mbognou, F. C. F.; El-Miad, A. K. The intensity and direction of the electric field effects on off-center shallow-donor impurity binding energy in wedge-shaped cylindrical quantum dots.*Thin Solid Films* **2022**, *757* , 139396,https://doi.org/10.1016/j.tsf.2022.139396.
10. Bejan, D.; Stan, C. Electron spin and donor impurity effects on the absorption spectra of pseudo-elliptic quantum rings under magnetic field.*Philosophical Magazine* **2021**,*101*, 1871-1893,https://doi.org/10.1080/14786435.2021.1939900.
11. Creffield, C. E.; Platero, G. Dynamicalcontrol of correlated states in a square quantum dot.*Phys.Rev. B***2002**, *66*, 235303,https://doi.org/10.1103/PhysRevB.66.235303.
12. Noba, K.-i. Dynamic localization of twoelectrons in a one-dimensional lattice system driven by anoscillating electric field. *Phys. Rev. B***2003**, *67*, 153102,https://doi.org/10.1103/PhysRevB.67.153102.
13. Platero, G.;Aguado, R.Photon-assistedtransport in semiconductor nanostructures. *Phys. Reports***2004**, *395*, 1-157,https://doi.org/10.1016/j.physrep.2004.01.004.
14. Paspalakis, E.; Terzis, A. F. Localization effects in a two-electron quantum dot molecule:The case of AC-DC driving fields. *J. Appl. Phys.***2004**, *95*,1603-1605,http://dx.doi.org/10.1063/1.1637723.
15. Paspalakis, E.;Terzis, A. F. Controlled excitonic population transfer in a quantum dotsystem interacting with an electromagnetic field: Localfield effects. Proceedings of the 5th WSEAS InternationalConference on Microelectronics, Nanoelectronics,Optoelectronics, Prague, Czech Republic,March 12-14,**2006**, https://journals.aps.org/prb/abstract/10.1103/PhysRevB.73.073305.
16. Paspalakis, E.; Kalini, A.; Terzis, A. F. Local field effects in excitonic population transfer ina driven quantum dot system. *Phys. Rev. B***2006**, *73*, 073305,https://doi.org/10.1103/PhysRevB.73.073305.
17. Paspalakis, E.; Simserides, C.; Terzis, A. F. Controlled intersubband population dynamicsin a semiconductor quantum well. *AIP Conference Proceedings***2007**, *963*, 533, https://doi.org/10.1063/1.2827038.
18. Paspalakis, E.; Simserides, C.; Baskoutas, S.; Terzis, A. F. Electromagnetically inducedpopulation transfer between two quantum well subbands.*Phys. E***2008**, *40*, 1301-1304,https://doi.org/10.1016/j.physe.2007.08.078.
19. Çakir, B.; Yakar, Y.; Özmen, A.; Sezer, M. Ö; Şahin, M. Linear and nonlinear optical absorption coefficients and binding energy of a spherical quantum dot. *Superlattices Microstruct.***2010,** *47*, 556-566,https://doi.org/10.1016/j.spmi.2009.12.002.
20. Yakar, Y.; Çakir, B.; Özmen, A. Magnetic field effects on oscillator strength, dipole polarizability and refractive index changes in spherical quantum dot. *Chem. Phys. Lett.* **2018**, *708*, 138-145,https://doi.org/10.1016/j.cplett.2018.08.010.
21. Kirak, M.; Yilmaz, S.; Şahin, M.; Gencaslan, M. The electric field effects on the binding energies and the nonlinear optical properties of a donor impurity in a spherical quantum dot. *J. Appl.Phys.* **2011,** *109*, 094309,https://doi.org/10.1063/1.3582137.

Commented [AGN8]: Please omit this reference as DOI number is not available

22. Kirak, M.; Yilmaz, S.; Temizer, Ü. Nonlinear optical rectification and oscillator strength in a spherical quantum dot with parabolic confinement in the presence of the electric field. *J. Nanoelectron. Optoelectron.***2013,** *8*, 165-169,https://doi.org/10.1166/jno.2013.1447.
23. Karabulut, I.; Atav, Ü.;Şafak, H.; Tomak, M. Linear and nonlinear intersubband optical absorptions in an asymmetric rectangular quantum well. *Euro. Phys. J. B* **2007,** *55*, 283-288,https://doi.org/10.1140/epjb/e2007-00055-1.
24. Aytekin, O.;Turgut, S.;Tomak, M. Nonlinearoptical properties of a Pöschl–Teller quantum well underelectric and magnetic fields.*Phys. E***2012**,*44*,1612-1616,https://doi.org/10.1016/j.physe.2012.04.005.
25. Khordad, R.; Bahramiyan, H. Impurity position effect on optical properties of various quantum dots. *Phys. E* **2015,** *66*, 107-115,https://doi.org/10.1016/j.physe.2014.09.021.
26. Restrepo, R. L.; Morales, A. L.;Martínez-Orozco, J. C.;Baghramyan, H. M.;Barseghyan, M. G.; Mora-Ramos, M. E.; Duque, C. A. Impurity-related nonlinearoptical properties in delta-doped quantum rings: Electricfield effects. *Phys. B***2014**, *453*, 140-145,https://doi.org/10.1016/j.physb.2014.05.004.
27. Bouzaiene,L.;Alamri,H.;Sfaxi,L.;Maaref,H. Simultaneous effects of hydrostatic pressure,temperature and electric field on optical absorption in*InAs/GaAs* lens shape quantum dot.*J. Alloys Compd.* **2016**,*655*, 172-177,https://doi.org/10.1016/j.jallcom.2015.09.181.
28. Liu, G.; Guo, K. –X.; Hassanabadi, H.; Lu, L. Linear and nonlinear optical properties in adisk-shaped quantum dot with a parabolic potential plus ahyperbolic potential in a static magnetic field. *Phys. B* **2012**, *407*, 3676-3682,https://doi.org/10.1016/j.physb.2012.05.049.
29. Li, B.; Guo, K. –X.; Liu, Z. –L.;Zheng, Y. –B. Nonlinear optical rectification in parabolic quantumdots in the presence of electric and magnetic fields. *Phys. Lett. A* **2008,***372*, 1337-1340,https://doi.org/10.1016/j.physleta.2007.09.075.
30. Rezaei, G.; Vahdani, M. R. K.; Vaseghi, B. Nonlinear optical properties of a hydrogenic impurity inan ellipsoidal finite potential quantum dot. *Current Appl. Phys.***2011**, *11*, 176-181,http://dx.doi.org/10.1016/j.cap.2010.07.002.
31. Rezaei, G.; Vaseghi, B.; Taghizadeh, F.; Vahdani, M. R. K.; Karimi, M. J.Intersubband opticalabsorption coefficient changes and refractive index changesin a two-dimensional quantum pseudodot system.*Superlattices Microstruct.***2010**, *48*, 450-457,https://doi.org/10.1016/j.spmi.2010.08.009.
32. Karimi,M. J.;Rezaei,G. Effects ofexternal electric and magnetic fields on the linear andnonlinear intersubband optical properties of finitesemi-parabolic quantum dots, *Phys. B* **2011,***406*, 4423-4428,https://doi.org/10.1016/j.physb.2011.08.105.
33. Ghazi, H. El.; Jorio, A.; Zorkani, I. Pressure-dependent of linear and nonlinear opticalproperties of *(In,Ga)N/GaN* spherical QD.*Superlattices Microstruct*. **2014**, *71*, 211-216,https://doi.org/10.1016/j.spmi.2014.03.046.
34. Ghazi, H. El.; Jorio, A.; Zorkani, I.Theoretical investigation of stark effect on shallow donor binding energy in *InGaN* spherical QD-QW, *Phys. B* **2013** ,*422* , 47-50,https://doi.org/10.1016/j.physb.2013.04.011.
35. Bejan, D.; Stan, C.;Niculescu, E.C. Opticalproperties of an elliptic quantum ring: Eccentricity andelectric field effects, *Opt. Mater.***2018**, *78*, 207-219,https://doi.org/10.1016/j.optmat.2018.02.008.
36. Kumar, K.M.; Peter, A.J.; Lee, C.W. Optical properties of a hydrogenic impurity in a confined $Zn_{1-x}Cd_xSe/ZnSe$ spherical quantum dot. *Superlattices Microstruct.* **2012,** *51*, 184-193,https://doi.org/10.1016/j.spmi.2011.11.012.
37. Ungan, F.;Bahar, M. K.;Barseghyan, M. G.; Pérez, L. M.;Laroze,D.; Effect of intense laser and electric fields on nonlinear optical properties of cylindrical quantum dot with Morse potential.*Optik* **2021**, *236*, 166621,https://doi.org/10.1016/j.ijleo.2021.166621.
38. Tuzemen, A. T.;Dakhlaoui, H.; Mora-Ramos, M. E.;Ungan, F. The nonlinear optical properties of *GaAs/GaAlAs* triple quantum well: Role of the electromagnetic fields and structural parameters, *Phys. B* **2022**,*646*, 414286,https://doi.org/10.1016/j.physb.2022.414286.
39. Tuzemen, A. T.; Mora-Ramos, M. E.;Ungan, F.; Investigation of linear and nonlinear optical absorption coefficients and refractive index changes of a zigzag quantum well with structure parameters and applied external fields. *Phys. B* **2022**,*647*, 414379,http://dx.doi.org/10.1016/j.physb.2022.414379.
40. Mantashian, G. A.;Zaqaryan, N. A.;Mantashyan, P. A.;Sarkisyan, H. A.;Baskoutas, S.;Hayrapetyan, D. B. Linear and nonlinear optical absorption of *CdSe/CdS* core/shell quantum dots in the presence of donor impurity. *Atoms* **2021**, *9*, 75,https://doi.org/10.3390/atoms9040075.

41. Máthé, L.;Onyenegecha, C. P.;Farcaş, A-A.;Pioraş-Ţimbolmaş, L-M.; Solaimani, M.;Hassanabadi, H. Linear and nonlinear optical properties in spherical quantum dots: Inversely quadratic Hellmann potential,. *Phys. Lett. A* **2021**,*397*,127262,https://doi.org/10.1016/j.physleta.2021.127262.
42. Ungan, F.;Bahar, M. K.; Rodríguez-Magdaleno, K. A.; Mora-Ramos, M. E.;Martínez-Orozco, J. C. Influence of applied external fields on the nonlinear optical properties of a semi-infinite asymmetric $Al_xGa_{1-x}As/GaAs$ quantum well.*Materials Science in Semiconductor Processing* **2021**, *123*, 105509,https://doi.org/10.1016/j.mssp.2020.105509.
43. Fakkahi, A.;Kirak, M.;Sali, A. Effect of impurity position and electric field on the optical absorption coefficients and oscillator strength in spherical multilayer quantum dot. *Eur. Phys. J. Plus* **2022**, *137*, 1-19,https://doi.org/10.1140/epjp/s13360-022-03279-1.
44. Datta, S.; Arif, Sk. Md.; Roy, D.; Ghosh, M.Pulsed field induced excitation in impurity doped quantumdot: Interplay with Gaussian white noise.*Phys. B* **2022**, *643*, 414163,https://doi.org/10.1016/j.physb.2022.414163.
45. Datta, S.; Arif, Sk. Md.; Roy, D.; Ghosh, M.Excitation dynamics among impurity doped quantum doteigenstates in a polychromatic field: Role of Gaussian whitenoise, *ChemistrySelect* **2022**, *07*, e202202244,https://doi.org/10.1002/slct.202202244.
46. Datta, S.; Arif, Sk. Md.; Roy, D.; Ghosh, M.Analyzing time-average excitation rate among quantum doteigenstates triggered by time-dependent noise strength. *Phys. Status Solidi B*(in press), https://doi.org/10.1002/pssb.202200216.
47. Rajashabala, S.; Navaneethakrishnan, K. Effects of dielectric screening and position dependent effective mass on donor binding energies and on diamagnetic susceptibility in a quantum well. *Superlattices Microstruct.***2008,** *43*, 247-261,https://doi.org/10.1016/j.spmi.2007.11.002.
48. Rajashabala, S.; Navaneethakrishnan, K. Effective masses for donor binding energies in quantum well systems. *Mod. Phys. Lett. B* **2006,** *20*, 1529-1541,https://doi.org/10.1142/S0217984906011633.
49. Peter, A.J.; Navaneethakrishnan, K. Effects of position-dependent effective mass and dielectric function of a hydrogenic donor in a quantum dot. *Phys.E***2008,***40*, 2747-2751,https://doi.org/10.1016/j.physe.2007.12.025.
50. Khordad, R.; Effects of position-dependent effective mass of a hydrogenic donor impurity in a ridge quantum wire. *Phys E* **2010,** *42*, 1503-1508, https://doi.org/10.1016/j.physe.2009.12.006.
51. Khordad, R.; Effect of position-dependenteffective mass on linear and nonlinear optical properties of a cubic quantum dot. Phys. B**2011**, *406*, 3911-3916,https://doi.org/10.1016/j.physb.2011.07.022.
52. Qi, X.-H.; Kang, X.-J.; Liu, J.J. Effect of a spatially dependent effective mass on the hydrogenic impurity binding energy in a finite parabolic quantum well. *Phys. Rev. B* **1998,** *58*, 10578-10582,https://doi.org/10.1103/PhysRevB.58.10578.
53. Peter, A.J. The effect of position-dependent effective mass of hydrogenic impurities in parabolic *GaAs/GaAlAs*quantum dots in a strong magnetic field. *Int. J. Mod. Phys. B* **2009,** *26*, 5109-5118,https://doi.org/10.1142/S0217979209053394.
54. Li, Y.-X.; Liu, J.-J.; Kang, X.-J. The effect of a spatially dependent effective mass on hydrogenic impurity binding energy in a finite parabolic quantum well. *J. Appl. Phys.* **2000,** *88*, 2588-2592,https://doi.org/10.1063/1.1286244.
55. Naimi, Y.; Vahedi, J.; Soltani, M.R. Effect of position-dependent effective mass on optical properties of spherical nanostructures. *Opt. Quant. Electron.* **2015,** *47*, 2947-2956,.https://doi.org/10.1007/s11082-015-0183-5.
56. Köksal, M.; Kilicarslan,E.; Sari,H.; Sökmen,I. Magnetic-field effect on the diamagnetic susceptibility of hydrogenic impurities in quantum well-wires, *Phys. B***2009**, *404*, 3850-3854,https://doi.org/10.1016/j.physb.2009.07.103.
57. Deng, Z.-Y.; Guo, J.-K.; Lai, T.-R. Impurity states in a spherical $GaAs.Ga_{1-x}Al_xAs$ quantum dot: Effects of the spatial variation of dielectric screening. *Phys. Rev. B* **1994,** *50*, 5736-5739,https://doi.org/10.1103/PhysRevB.50.5736.
58. Xie, W. Third-order nonlinear optical susceptibility of a donor in elliptical quantum dots. *Superlattices Microstruct.***2013,** *53*, 49-54,https://doi.org/10.1016/j.spmi.2012.09.009.
59. Xie, W. Optical anisotropy of a donor in ellipsoidal quantum dots. *Phys. B* **2012,** *407*, 4588-4591,https://doi.org/10.1016/j.physb.2012.08.023.
60. Safarpour, Gh.; Izadi, M.A.; Novzari, M.; Niknam, E.; Moradi, M. Anisotropy effect on the nonlinear optical properties of a three-dimensional quantum dot confined at the center of a cylindrical nano-wire. *Phys. E* **2014,** *59*, 124-132,https://doi.org/10.1016/j.physe.2014.01.007.

61. Safarpour, Gh.; Izadi, M.A.; Novzari, M.; Yazdanpanahi, S. Anisotropy effect on the linear and nonlinear optical properties of a laser dressed donor impurity in a *GaAs/GaAlAs* nanowire superlattice. *Superlattices Microstruct.***2014,** *75*, 936-947,https://doi.org/10.1016/j.spmi.2014.09.018.
62. Karki, H.D.; Elagöz, S.; Başer, P. Simultaneous effects of hydrostatic pressure and temperature on the binding energy of hydrogenic impurity in cylindrical quantum well wires. *Superlattices Microstruct.***2010,** *48*, 298-304,https://doi.org/10.1016/j.spmi.2010.06.021.
63. Lu, L.; Xie, W.; Shu, Z. Combined effects of hydrostatic pressure and temperature on nonlinear properties of an exciton in a spherical quantum dot under the applied electric field. *Phys. B* **2011,** *406*, 3735-3740,https://doi.org/10.1016/j.physb.2011.06.081.